Stretched exponential dynamics in lipid bilayer simulations

Erik G. Brandt[a] and Olle Edholm[b]
Theoretical Biological Physics, Department of Theoretical Physics, Royal Institute of Technology, AlbaNova University Center, SE-106 91 Stockholm, Sweden

(Received 11 May 2010; accepted 23 July 2010; published online 16 September 2010)

The decay of fluctuations in fluid biomembranes is strongly stretched and nonexponential on nanometer lengthscales. We report on calculations of structural correlation functions for lipid bilayer membranes from atomistic and coarse-grained molecular dynamics simulations. The time scales extend up to microseconds, whereas the linear size of the largest systems is around 50 nm. Thus, we can cover the equilibrium dynamics of wave vectors over two orders of magnitude ($0.2-20\ \mathrm{nm}^{-1}$). The time correlations observed in the simulations are best described by stretched exponential functions, with exponents of 0.45 for the atomistic and 0.60 for the coarse-grained model. Area number density fluctuations, thickness fluctuations, and undulations behave dynamically in a similar way and have almost exactly the same dynamics for wavelengths below 3 nm, indicating that in this regime undulations and thickness fluctuations are governed by in-plane density fluctuations. The out-of-plane height fluctuations are apparent only at the longest wavelengths accessible in the simulations (above 6 nm). The effective correlation times of the stretched exponentials vary strongly with the wave vector. The variation fits inverse power-laws that change with wavelength. The exponent is 3 for wavelengths smaller than about 1.25 nm and switches to 1 above this. There are indications for a switch to still another exponent, 2, for wavelengths above 20 nm. Compared to neutron spin-echo (NSE) experiments, the simulation data indicate a faster relaxation in the hydrodynamic limit, although an extrapolation of NSE data, as well as inelastic neutron scattering data, is in agreement with our data at larger wave vectors. © *2010 American Institute of Physics*. [doi:10.1063/1.3478998]

I. INTRODUCTION

The dynamics of simple liquids is described by the density-density correlation function, $G(r,t)$, first introduced by van Hove[1] in 1954. Liquid state theories are usually formulated in terms of its Fourier transform in space, $F(q,t)$ (intermediate scattering function), or its Fourier transform in space and time, $S(q,\omega)$ (dynamic structure factor).[2] Simple expressions for these functions can be obtained by solving the linearized (Navier–Stokes) hydrodynamic equations,[2,3] with the result that the long-time dissipative decay of the density correlation function is exponential in time, corresponding to a Lorentzian peak in the Fourier spectrum $S(q,\omega)$. The spectrum also contains two additional side peaks due to inelastic scattering from propagating sound waves, which correspond to rapidly damped oscillations in time. This famous structure is known as the Rayleigh–Brillouin triplet and is valid on hydrodynamic time and length scales that are far greater than the distance between neighboring particles in the liquid. In dynamic light scattering experiments, which probe large wavelengths, the three peaks are well separated but at shorter distances, as probed in neutron and x-ray scattering and in molecular dynamics (MD) simulations, the picture is more complex. As the continuum approximation starts to break down, the hydrodynamic dispersion relations become invalid and the peaks overlap. An attempt to extend the domain of validity of continuum hydrodynamics down to molecular scales is provided by generalized hydrodynamic theory, which introduces nonlocal (time- and space-dependent) transport coefficients in the hydrodynamic equations. The approach is in essence phenomenological but provides a framework wherein the time correlation formalism has been rigorously studied.[4] The limitations of the Rayleigh–Brillouin triplet structure were clear already at an early stage,[5] as additional contributions to $S(q,\omega)$ were observed both for simple and complex fluids.[4] To give a well known example, the Rayleigh peak of liquid glycerol was better fitted to two Lorentzians,[6,7] which would correspond to a time decay by two exponentials. Many models have been suggested to improve the classic hydrodynamic result and the literature on the subject is rich. For a recent overview, see, e.g., Bafile and co-workers[8] and the references therein.

In molecular liquids, internal degrees of freedom contribute to the dynamics and can cause correlations to remain over many orders in time. Lipid bilayers are even more complex as the lipid/water interface introduces an additional contribution to the relaxation dynamics. The lipid bilayer may be viewed as a thin fluid sheet that is surrounded by water on both sides. This allows for not only definitions of other types of time correlation functions (with corresponding dynamic structure factors), including undulations of the entire thin sheet, but also thickness fluctuations of the bilayer. The static properties of these modes are fairly well understood[9] and some efforts to describe and simulate the dynamics of such

[a]Electronic mail: erbr02@kth.se.
[b]Electronic mail: oed@kth.se.

motions have been undertaken.[10] Computer simulations, in particular, have been severely hampered by the relatively long time scales involved with such motions.

The internal molecular structure of the bilayer also gives rise to orientation fluctuations of the fatty acid chains that build up the bilayer hydrophobic core. These motions can be monitored by nuclear magnetic resonance (NMR) methods and clearly indicate a slow (most likely) algebraic ($t^{-1/2}$) decay of the correlations functions[11] although the experimental resolution is limited by the need of NMR-machines operating at widely different low magnetic fields. Simulations[12,13] support a slow decay and can be fitted to algebraic decay, as well as to a stretched exponential or at least four exponentials. The fluctuations in orientation behind this decay are more local than the dynamics of the long-wavelength Fourier modes studied in the present article. Still there is a strong similarity in the stretched behavior of the correlation functions. The fast short-time dynamics, reflected in the Brillouin peaks, is a separate problem that has been addressed in an earlier study by the present authors.[14] That work not only indicated that generalized hydrodynamics work quite well in this regime but also pointed to some differences compared to the classical dispersion relations.

In this paper, the focus is put on the long time dynamics reflected in the central Rayleigh peak of the dynamic structure factor. The aim is to push the simulations toward small wave vectors, which requires large system sizes and long simulation times since the decay times of the correlation functions increase substantially with distance. Present computer power makes it possible to cover wave vectors down to $q=0.2-0.3$ nm^{-1} and opens up the possibility to directly compare simulation data to recent experimental neutron spin-echo (NSE) data.[15–17] Earlier simulation studies, of a coarse-grained model[18,19] and of an atomistic model,[20] were interpreted in different theoretical frameworks and have either covered a very narrow q-range or only included single-particle motions. The present work investigates a broad set of wave vectors and includes the full collective motion of the bilayer so that all the relevant dispersion relations can be extracted from the wave vector-dependence of the decay of the correlation functions. In addition, both atomistic and coarse-grained simulations are performed and the timescales are mapped to allow for comparison between the different simulations.

To help in the interpretation of experimental (and simulation) data, many theories have been proposed that mainly differ in geometric details, but also take different prerequisites for the bilayer structure. They support time correlation functions that can be described either by multiple or stretched exponentials, including the two-exponential theories of Seifert and Langer[21,22] and Evans and Yeung[23,24] for the dynamics of membrane undulations. The calculations of these models are involved and in the end the amplitude of a single exponential dominates in the q-range covered by the present simulations. Zilman and Granek[25,26] have put forward a powerful theory that predicts stretched exponential decay for the density fluctuations, with exponent $\beta=2/3$ for all q, and a dispersion relation that scales as $t_0 \propto q^{-3}$. We will show that this fits the present data to some extent but there

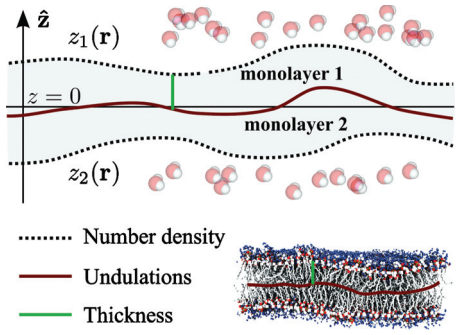

FIG. 1. The bilayer (gray) embedded in water (not shaded), where the surfaces $z_1(x,y)$ and $z_2(x,y)$ represent the monolayers [and $z_1(x,y)>z_2(x,y)$]. Number densities are considered as projections in the lateral plane.

are also important differences that so far have not been reported. Stretched time correlation functions have been reported in a number of complex systems but of particular interest to bilayer dynamics, in polymer systems,[27] and in glass-forming liquids.[28,29] Whether the origin of the stretching is universal is far from certain and a unifying description of the behavior is still lacking. One purpose of this paper is to investigate the different contributions to the relaxation dynamics in lipid bilayer simulations and shed some more light on the origin of the stretched time correlation functions.

II. THEORY

A. The bilayer structure

In the analysis of the atomistic simulation data, the bilayer is represented as two surfaces $z_1(x,y)$ and $z_2(x,y)$ $(z_1>z_2)$, calculated from the phosphate atoms of the two monolayers (Fig. 1). The linear combinations,

$$u(x,y)=\tfrac{1}{2}(z_1(x,y)+z_2(x,y))$$

and

$$h(x,y)=\tfrac{1}{2}(z_1(x,y)-z_2(x,y)), \tag{1}$$

describe the undulating average surface and half the bilayer thickness, respectively.

The local area number density is defined as

$$\rho(x,y)=\tfrac{1}{2}(\rho_{1_\parallel}(x,y)+\rho_{2_\parallel}(x,y)), \tag{2}$$

where $\rho_{j_\parallel}(x,y)$ are monolayer number densities projected into the lateral plane. A Fourier expansion of the surfaces $j=1,2$ is introduced as

$$z_j(\mathbf{r})=\sum_{\mathbf{q}} \hat{z}_j(\mathbf{q})e^{i\mathbf{q}\cdot\mathbf{r}}$$

with

$$\hat{z}_j(\mathbf{q})=\frac{1}{A}\int \mathrm{d}^2\mathbf{r} z_j(\mathbf{r})e^{-i\mathbf{q}\cdot\mathbf{r}}. \tag{3}$$

The Fourier coefficients of the two monolayer surfaces are now obtained from the time-dependent coordinates $\mathbf{r}_{jn}(t)$ of the head group phosphate atoms as

$$\hat{z}_j(\mathbf{q},t) = \frac{1}{N_j}\sum_{n=1}^{N_j} z_{jn}(t)e^{-i\mathbf{q}\cdot\mathbf{r}_{jn}(t)}, \tag{4}$$

where the sum goes over all $n=1,N_j$ with $j=1$ or 2. The use of other atoms or averages of other atomic positions to define the surfaces give similar results. We have then

$$\hat{u}(\mathbf{q},t) = \frac{1}{2N}\sum_{n=1}^{N} \{z_{1n}(t)e^{-i\mathbf{q}\cdot\mathbf{r}_{1n}(t)} + z_{2n}(t)e^{-i\mathbf{q}\cdot\mathbf{r}_{2n}(t)}\}, \tag{5a}$$

$$\hat{h}(\mathbf{q},t) = \frac{1}{2N}\sum_{n=1}^{N} \{z_{1n}(t)e^{-i\mathbf{q}\cdot\mathbf{r}_{1n}(t)} - z_{2n}(t)e^{-i\mathbf{q}\cdot\mathbf{r}_{2n}(t)}\}, \tag{5b}$$

$$\hat{\rho}(\mathbf{q},t) = \frac{1}{2N}\sum_{n=1}^{N} \{e^{-i\mathbf{q}\cdot\mathbf{r}_{1n}(t)} + e^{-i\mathbf{q}\cdot\mathbf{r}_{2n}(t)}\}, \tag{5c}$$

with the number of lipids per monolayer equal ($N_1=N_2=N$), a simple but by no means necessary specialization. The functions $u(\mathbf{r},t)$, $h(\mathbf{r},t)$, and $\rho(\mathbf{r},t)$ are real, which means that their Fourier coefficients fulfill the relations $\hat{u}(\mathbf{q},t) = \hat{u}^*(-\mathbf{q},t)$, $\hat{h}(\mathbf{q},t)=\hat{h}^*(-\mathbf{q},t)$, and $\hat{\rho}(\mathbf{q},t)=\hat{\rho}^*(-\mathbf{q},t)$. Periodic boundary conditions restrict the wave vectors to $\mathbf{q}=2\pi(n/L_x,m/L_y)$, with $n,m=\pm1,\pm2,\ldots$. The total projected area of the bilayer is denoted $A_\parallel$ and is equal to L_xL_y. The periodic boundaries minimize edge effects, but do introduce a low-q cutoff $q_{\min}=2\pi/L_{\max}$ on the wave vectors. $L_{\max}$ depends on the size of the simulated system but is in practice limited to the order of 20–50 nm. This gives $q_{\min}$ $\sim$0.2–0.3 nm^{-1}, and even a tenfold increase of the linear lateral system dimension (100-fold increase in the number of atoms) reduces $q_{\min}$ to $\sim$0.03 nm^{-1}. Thus, only a fairly small number of Fourier modes is available in the region where the continuum description is expected to be valid (below $\sim$2 nm^{-1}), even in the largest state-of-the-art computer simulations including thousands of lipids. We tacitly remove the time and space independent components, u_0 for the undulations (which can be put to zero by a proper choice of coordinate system), h_0 half the bilayer thickness and $\rho_0 = N/A = a_0^{-1}$, the average area number density, and focus on the fluctuations. Time autocorrelation functions can now be defined as

$$F_a(q,t) = \langle \hat{a}(\mathbf{q},t)\hat{a}^*(\mathbf{q},0)\rangle, \tag{6}$$

with a being u, h, or ρ. Here, we assume that these functions depend only on the magnitude of the wave vector not on its direction. This follows from the isotropy of the system in the lateral plane, but could be affected by the rectangular periodic boundary conditions. Simulation data indicate that such anisotropy vanishes given enough frames in the averaging (data not shown).

$F_\rho(q,t)$ may be identified with the intermediate scattering function in liquid state theory,[2,4] i.e., the spatial Fourier transform of the density-density autocorrelation function of a bulk liquid. However, since the lipid bilayer may be viewed as a two-dimensional liquid embedded in a three-dimensional liquid (water), there are two sources of the structural fluctuations in a free floating lipid bilayer. First, there are shape fluctuations of the bilayer interface, mainly from molecular collisions of water with the monolayer surfaces. Second, there are fluctuations in the bulk of the fluid bilayer, from thermal motions of lipid molecules. This infers that $F_u(q,t)$ and $F_h(q,t)$ include contributions from fluctuations in the shape of the interface as well as from the bulk, while $F_\rho(q,t)$ only probes the later fluctuations. An important objective is to explore the intertwining of these contributions on different length scales.

For every Fourier mode q, the correlation function $F_a(q,t)$ may be characterized by a relaxation time $\tau_a(q)$ that measures the correlation length. $\tau_a(q)$ is here defined following Refs. 30–32, from the integral of the squared correlation function as

$$\tau_a(q) = 2\int_0^\infty \mathrm{d}t \frac{[F_a(q,t)]^2}{[F_a(q,0)]^2}. \tag{7}$$

A straightforward integration (without squaring) is also a perfectly viable definition with its own advantages. In the following sections the a-subscript on $\tau(q)$ and $F(q,t)$ is suppressed when there is no risk of ambiguity.

TABLE I. The different simulations. N_L is the number of lipids, T the (unscaled) simulation time, and a_0 is the projected area per lipid obtained from constant pressure simulations with an error estimate in parenthesis for the last digit.

Force field[a]	N_L	T (μs)	a_0[b] (nm^2)
UA	128	1.000	0.61(1)
UA	1024	1.000	0.605(4)
CG	1024	2.000	0.587(4)
CG	8192	2.000	0.587(2)

[a]UA=United-atom force field (Ref. 35). CG=Coarse-grained force field (Refs. 36–38) as described in Sec. III B in the text.
[b]The current experimental value from Ref. 34 is 0.606(5) nm^2 for DMPC at 303 K.

III. METHODS

A. Preparation of systems

A lipid bilayer was constructed starting from the atomic coordinates of the unit cell of crystal structure 1,2-dimyristoyl-sn-glycero-3-phosphocholine (DMPC, 14:0),[33] which contains 2×2 molecules in bilayer shape. The unit cell was replicated in the lateral directions resulting in a bilayer membrane containing 64 molecules (32 in each monolayer). The in-plane coordinates were rescaled to commensurate with a recent experimental number, $a_0 = 0.606\pm0.005$ nm^2, for the area per lipid in the fluid L_α-phase.[34] The structures were energy minimized to remove possible steric atomic overlaps in the bilayers, and then hydrated with 23 waters per lipid. This was followed by an additional energy minimization before equilibration simulations were carried out for 100 ns, to make sure that all dynamic modes in the system had time to fully develop. All simulation systems reported in this work were created by replication of the described template structures and are summarized in Table I.

B. Force fields

Two force fields were used to model the lipid and water molecules, chosen to represent different (but overlapping) levels of detail of the bilayer structure. The first was the "united-atom" (UA) force field of Berger and co-workers[35] which is atomistic except for nonpolar hydrogens, which are included into single-particle beads for CH, CH_2, and CH_3 groups. Water is included explicitly with the Simple Point Charge (SPC) water model.[39] The Berger force field is well known to reproduce structural[40] and dynamical quantities[12,13] of phospholipid bilayers. To enable simulations of larger systems for longer times, the "coarse-grained" (CG) MARTINI 2.1 force field[36–38] was also used. This four-to-one-mapping (four heavy atoms are replaced with one interaction center) of the atomistic model leaves the representation of the 14 carbon groups in the fatty acid chain of DMPC open to either three or four particle beads in MARTINI. Three beads correspond to 12 carbons, which is 1,2-dilauroyl-sn-glycero-3-phosphocholine (DLPC 12:0), while four beads correspond to 16 carbons, i.e., 1,2-dipalmitoyl-sn-glycero-3-phosphocholine (DPPC 16:0). We chose DLPC, but at the CG level of modeling the DMPC/DLPC versus DPPC/DLPC distinction should not be crucial.

Waters are incorporated in the MARTINI force field as van der Waals-spheres and represent four real water molecules each. As discussed in one of the original papers,[37] this water model suffers from a too high freezing point (280–300 K depending on simulation conditions). A small amount of counterpoising antifreeze agent in the bulk water (~10%) lowers the freezing point. Although the MARTINI force field convincingly reproduces structural properties of lipid bilayers, it is less certain to which extent it correctly reproduces the dynamical properties. The coarse-graining of the lipids means that phase space is smoothened so that the simulation dynamics becomes faster than the "true" dynamics. The original papers estimated this difference from the diffusion coefficient of water and found it to be a factor of 4. It is not obvious that the same scaling can be applied to lipid bilayers. Comparing correlation times between the UA and CG models, we estimate an average scaling factor of 10. All times reported from the CG simulations here are scaled by this factor unless stated explicitly otherwise.

C. Simulation parameters

MD simulations were performed on all systems with the GROMACS (Ref. 41) 4 program, using a leap-frog Verlet algorithm to integrate the equations of motion. To determine when a simulation was equilibrated, the potential energy and the area per lipid were monitored. In addition, the Fourier amplitudes at the lowest wave vectors ($q < 1$ nm^{-1}) of the undulation spectrum were plotted at regular times. When the amplitudes did not change, the system was considered to be in equilibrium and the equilibration data were discarded. The production simulation was then run for the total times reported in Table I. All simulations were run in parallel on a supercomputer cluster with 2 Quad-Core CPU:s per node, with the systems prepared in the isothermal-isobaric (NPT) ensemble at constant temperature and pressure, corresponding to 300 K and 1 bar, respectively.

The following parameters were specific to the UA simulations. The time integration was performed with a 4 fs time step, with atom bonds constrained by the P-LINCS algorithm.[42] A neighbor list, recalculated every tenth step, was used up to 1.0 nm and a cutoff at 1.0 nm was applied for nonbonded interactions. Van der Waals interactions were simply truncated at this distance, whereas electrostatic interactions were calculated directly in real space up to the cutoff, and in Fourier space beyond, with Ewald summation using particle mesh ewald (PME).[43,44] The grid spacing in the PME algorithm was set to 0.12 nm. A Nose–Hoover thermostat[45,46] with a time constant of 0.5 ps was used to control the ensemble temperature, while an analog Parrinello–Rahman barostat[47,48] with a time constant of 50 ps was used to keep the pressure fixed. The lipids and the water were coupled to independent thermostats to avoid unwanted heating/cooling artifacts. For the barostat, the lateral box dimensions were coupled independently of the normal dimension to the pressure of 1 bar, to give a tensionless bilayer.

For the CG simulations essentially the original parameters were used. The integration time step was 40 fs. Nonbonded interactions were included by Coulomb and Lennard-Jones potentials, with energies and forces shifted to smoothly approach zero at the cutoff. The Lennard-Jones interactions were shifted from 0.9 nm to vanish at 1.2 nm, while the Coulomb interactions were shifted in the entire range up to 1.2 nm. Explicit charge screening were included by scaling the electrostatic interactions with a relative dielectric constant $\epsilon_r = 15$. A neighbor list with a range of 1.2 nm was set up and regenerated every tenth simulation step, whereas the ensemble temperature and pressure were controlled at the same state point (300 K and 1 bar) and in the same way as for the UA simulations but with different time constants, 2.5 ps for the thermostat and 250 ps for the barostat.

D. Calculation of time correlation functions from MD simulations

The time autocorrelation function of a dynamical variable $a(t)$ is

$$F(t) = \lim_{T\to\infty} \frac{1}{T} \int_0^T \mathrm{d}t_0 a(t_0 + t) a(t_0), \tag{8}$$

as an average over all initial times. Since the integral in Eq. (8) is a convolution integral, the Fourier transform of the time correlation function is obtained as

$$\hat{F}(\omega) = |\hat{a}(\omega)|^2. \tag{9}$$

$F(t)$ is then obtained by inverse transformation. Fast Fourier transform techniques make this calculation very efficient (see, e.g., Ref. 49). The statistical error in the correlation function is obtained as[30–32]

$$\Delta(t) = \sqrt{\frac{2\tau}{T}}(F(0) - F(t)), \tag{10}$$

assuming that $a(t)$ is a random Gaussian variable and $F(t \to \infty) = 0$. Here τ is the correlation time defined in Eq. (7) and T the total simulation time. Thus, 1% precision in the correlation function requires a simulation for $2 \times 10^4 \tau$. For Fourier components, the situation is slightly improved since the system is isotropic, by averaging over the magnitude of the wave vector $q = |\mathbf{q}|$. N_q wave vectors in the interval $q \pm \Delta q$ include an additional factor $N_q^{-1/2}$ into the right side of Eq. (10). This is due to that this situation is roughly equal to that of N_q systems containing a single (same) Fourier mode. The interval $\Delta q = 0.1$ nm^{-1} was used in this work with a resulting $N_q \sim 1$ for the lowest wave vectors to $N_q \sim 100$ for the largest wave vectors. The correlation functions were calculated for all Fourier modes and then averaged by binning over Δq.

E. Simulation data fitting and goodness-of-fits

The fitting of simulation data to analytical functions was done with a Levenberg–Marquardt algorithm,[50,51] implemented in a C program using the levmar library.[52] The entire data sets were used in the fits, which were done independently for each (fixed) value of q to obtain the dependency of the fit parameter upon the wave vector. Asymptotic error estimates, obtained from the diagonal elements of the fit covariance matrix, were clear underestimates and thus not used. Instead the noise in the fit between adjacent wave vectors was taken as a measure of the statistical accuracy of the fit. The goodness-of-fit of simulation data to a given model function (mf) was defined by

$$\epsilon_{\mathrm{mf}}(q) = \frac{\int_0^\infty \mathrm{d}t[F_{\mathrm{mf}}(q,t) - F(q,t)]^2}{\int_0^\infty \mathrm{d}t[F(q,t)]^2} \equiv \frac{\Delta\tau(q)}{\tau(q)}, \tag{11}$$

where $F(q,t)$ is the structure function calculated from simulation data and $F_{\mathrm{mf}}(q,t)$ is the fit of simulation data to that model function. Then $\tau(q)$ is the correlation time as defined in Eq. (7) and $\Delta\tau(q)$ is a measure of the quality of the fit. The division by $\tau(q)$ in Eq. (11) gives an error quantity that is dimensionless, independent of the shape of the model function, and provides a means to tell on which length scales the fit makes sense. In practice it was necessary to put a high-limit cutoff on the time integrals to exclude the influence of statistical noise. We truncated the integrations when the correlation functions had decreased to 5% of the initial value. We varied this value to include both more and less of the correlation function but the conclusions were firm in all cases even though the noise levels changed.

IV. RESULTS

The simulation results are presented in form of plots of the dynamic structure functions, Eq. (6), in Fig. 2 and the adjunct correlation times, Eq. (7), in Fig. 3. In the same manner as before $F(q,t)$ refers to any of the three functions, with $\tau(q)$ being the corresponding (wave vector-dependent) correlation time. Simulations were carried out on several system sizes for both force fields (Table I) but no systematic size effect on the correlation functions or the correlation times could be seen. Comfortingly, calculations from different system sizes for the same wave vectors matched. This check is especially important for the dynamics of the largest wavelengths in the simulation box, which could be affected by the periodic boundary conditions. To maintain clarity in plots, and keeping the ability to probe the smallest wave vectors, results are only reported from the simulations of the largest systems; the 1024-lipid system (UA-1024) for the united-atom simulations and the 8192-lipid system (CG-8192) for the coarse-grained simulations.

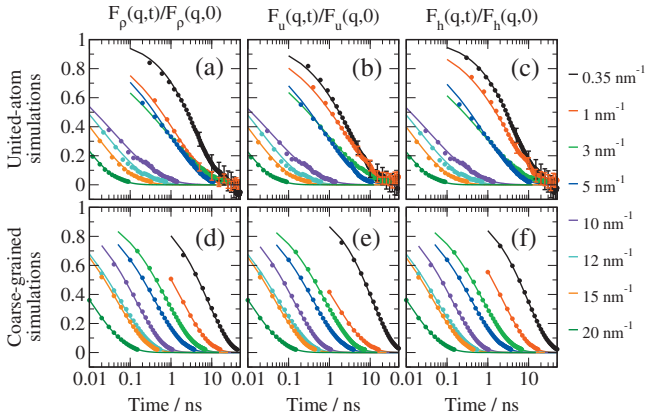

FIG. 2. The dynamic structure functions, $F_\rho(q,t)$ [(a) and (d)], $F_u(q,t)$ [(b) and (e)], and $F_h(q,t)$ [(c) and (f)] calculated from UA [(a)–(c)] and CG [(d)–(f)] simulations, at wave vectors between 0.35 and 20 nm^{-1}. Circles are simulation data (only a subset of data points are shown for clarity), error bars have been omitted when smaller than symbols. Solid lines are fits to stretched exponentials (see text). Times are reported in the physical time scale.

A. The shape of the time correlation functions

The dynamic structure functions are plotted in Fig. 2. They are remarkably similar in shape, with the most important feature, and the major result of this paper, being a non-exponential decay for the long times. Autocorrelation functions of Markovian processes, i.e., where the relaxation is

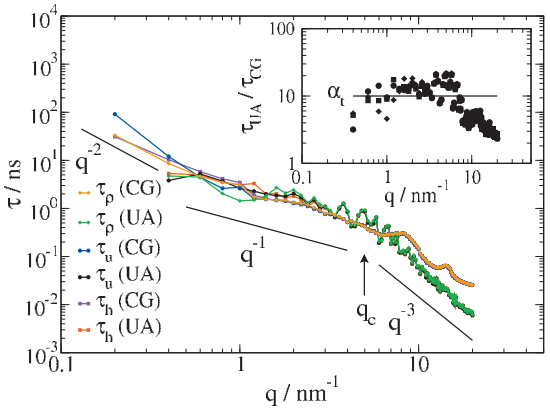

FIG. 3. $\tau(q)$ obtained from numerical integration of simulation data (filled circles). The solid lines between data points are guides to the eye. The power-law behaviors have been emphasized in black lines with the cross-over wave vector $q_c = 5$ nm^{-1} marked by an arrow. Times are reported in the physical timescale. Inset: The quotients between the correlation times for the UA and CG simulations can be used to obtain a factor α_t for mapping the time scales (see text). Data points are for τ_ρ (circles), τ_u (squares), and τ_h (diamonds).

memoryless, are exponentials with damping rates that depend on the wave vector. This implies that on the length scales probed by the simulations, 0.2–20 nm^{-1}, the relaxation of the membrane modes depends on previous times. A close inspection of the correlation functions in Fig. 2 reveals an early decay that is faster than for the intermediate and long times. Due to that the initial slope of the correlation functions must be zero to fulfill the thermodynamic sum rules,[4] Gaussian behavior is expected and found to be a good representation in this time regime. In principle, any function that is to represent the correlation functions for all times is required to interpolate between an initial Gaussian behavior to a gradually slower decay. Such functional forms have been suggested and their properties have been described.[53] Here, we note that this initial picosecond relaxation is due to fast vibration modes that are decoupled from the modes of structural relaxation. This paper focuses on the stretched decay on intermediate and longer times connected to the structural relaxation, and the short-time dynamics is ignored. The vibration modes, in particular, have been studied in earlier work[14] and can be expressed as propagating sound waves in the membrane. These sound waves damp out quickly and can be treated within a generalized hydrodynamic description, conventionally used for the relaxation dynamics in simple liquids.[2]

Both the UA and CG simulation data show that the correlations for the density, the undulations, and the thickness die out on the nanosecond timescale. Even at the lowest wave vectors, $q<1$ nm^{-1}, the autocorrelation functions decrease below the statistical accuracy within 100 ns. The statistical errors in the time correlation functions obtained from simulations are proportional to τ and increase with time [Eq. (10)]. Subsequently the correlation functions at long times were calculated with a precision ranging from at best 1% for the higher wave vectors to about 10% for the lowest wave vectors. In practice this means that in the best case the simulation data are statistically significant until the correlation function has decreased to ~1% but for the lowest wave vectors this number goes up to ~10%. Detecting, e.g., algebraic decays at the longest times are outside the precision reach of the present data. The data analysis was restricted to the time interval where the statistical uncertainty was below 10%.

B. The relaxation time

The correlation time $\tau(q)$ is model function-independent with the present definition [Eq. (7)] and was calculated by numerical integration of the simulation data at the different wave vectors. Cumulative summations were performed to ensure that the time integrals had converged and the influence of statistical noise kept to minimum. Figure 3 shows $\tau(q)$ from the UA and the CG simulations, as functions of wave vectors. $\tau(q)$ falls in the nanosecond regime, crossing over to picoseconds for the higher wave vectors, $q \gtrsim q_c = 5$ nm^{-1}. The curves are very similar for the UA and CG simulations down to 0.3 nm^{-1}, which is the limit of the UA data. The larger system size of the CG simulation data includes a few additional modes at lower q, down to 0.2 nm^{-1}. The decay of fluctuations is expected to slow down as the hydrodynamic limit ($q \to 0$) is approached as local excess must be physically transported to domains with local deficit, which will take an infinite time in a system of infinite size. The simulation data show that this regime has not been reached even at 0.3 nm^{-1}. The correlation times for the lowest modes of the CG data increase substantially but there are too few points to accurately determine any power-law behavior.

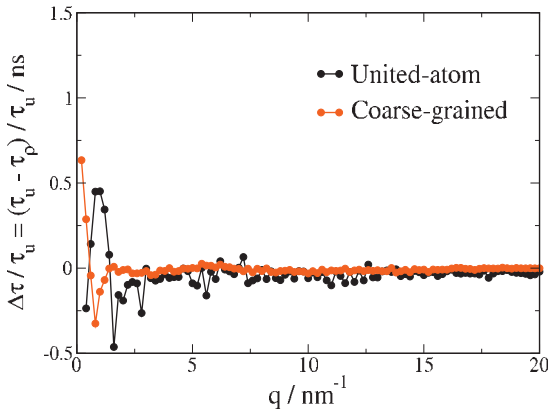

FIG. 4. Difference (normalized) between the correlation times for the undulations and the number density in the UA and CG simulations. Above $q_0 \approx 2$ nm^{-1} the correlation times are practically identical.

The factor α_t that maps the UA and CG timescales was determined by dividing the correlation times obtained for the two force fields (inset of Fig. 3). The quotient varies between 5 and 20 over the entire wave vector domain so the choice is to some degree arbitrary. An average over all wave vectors give $\alpha_t = 7 \pm 5$, but we have chosen a slightly higher value $\alpha_t = 10$ to obtain the best agreement in the mesoscopic wave vector regime 0.3–5 nm^{-1}. The price we pay is that the scaled CG dynamics at higher wave vectors is slightly slower than for the UA simulations. We note that α_t compares favorably to the interval of 2–10 suggested by the Martini authors based on comparison of diffusion coefficients between CG and UA simulations.[37]

Lipid bilayers relax as a combination of fluctuations in the membrane bulk and fluctuations of the membrane interface. To investigate the intermutual strength of the two contributions, the relaxation time of the density fluctuations (the in-plane two-dimensional structure) was compared to that of the undulations and thickness fluctuations, respectively. Strikingly, above $q = q_0 \approx 2$ nm^{-1}, the correlation times of both the undulations and the thickness coincide very closely to that of the number density (Fig. 4). The simplest interpretation is that for wave vectors above q_0 (distances shorter than ~3 nm) bulk fluctuations dominate. This corresponds to a spatial regime where $g(r)$, the radial distribution function, of the two-dimensional liquid differs from 1 (Fig. 5). In the vicinity of q_0 bulk fluctuations intertwine with fluctuations of the bilayer interface (undulations), and at even lower wave vectors (<1 nm^{-1}), the contributions start to separate. The simulation data do not reach q-values low enough to clearly enable a separation between bulk and interface fluctuations. The lowest q-modes of the CG simulations, inaccessible to the UA simulations, point to a relation between the number density and the thickness (implying fluctuations

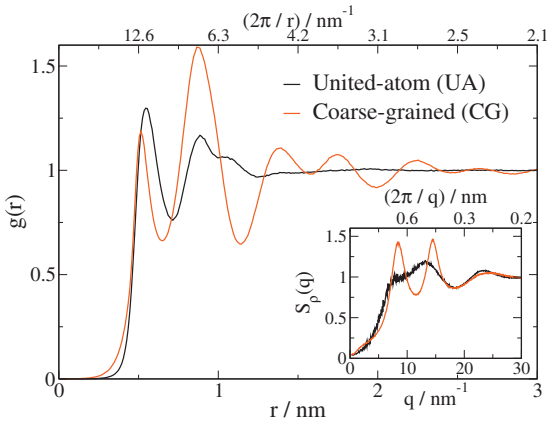

FIG. 5. The radial distribution function for the phosphorus atoms/particles in the UA and CG force fields. $g(r)$ approaching unity corresponds to that the number density is the same as that of the bulk. On the horizontal axis the radial coordinate is labeled below the figure and its inverse is labeled above the figure. Inset: The static structure factor $S_\rho(q)$ is the Fourier transform of $g(r)$. The wave vector and its inverse are given below and above the inset, respectively.

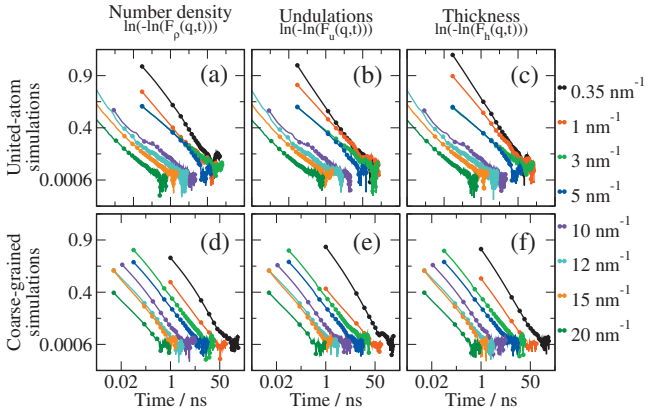

FIG. 6. UA [(a)–(c)] and CG [(d)–(f)] simulation data are linear when plotted as $\ln(-\ln(F(q,t)))$ against $\ln(t)$, a characteristic of the stretched exponential function. The behavior is very similar for the number density [(a) and (d)], the undulations [(b) and (e)], and the thickness [(c) and (f)]. The filled circles are simulation data and some points have been omitted for clarity. The solid lines are guides to the eye. Times are reported in the physical timescale.

at constant volume), while the undulations still grow. Nevertheless, the correlation times for undulations, thickness, and number density are similar over the entire range of wave vectors accessible by simulations.

The correlation times can be fitted to inverse power-laws in separate regimes (see Fig. 3). Up to q_c we find the exponent 1, and above it shifts to 3. The crossover is similar for the two force fields and occurs at a corresponding wavelength of 1.25 nm, i.e., slightly larger than the lipid neighbor distance. Possibly there is another regime in the low q-domain below 0.4 nm^{-1}, with an exponent close to 2 (see Fig. 3), but we have very few points in this regime and it is therefore difficult to draw any certain conclusions about this matter. A visible difference between the UA and CG simulation data is seen as peaks in the CG correlation times. The peak positions at 8 and 14 nm^{-1} coincide with the peaks in the static structure factor of the Martini model (Fig. 5),

$$S_\rho(q) = \langle \hat{\rho}(\mathbf{q})\hat{\rho}^*(\mathbf{q})\rangle, \tag{12}$$

which is an equilibrium property related to the initial value of the time correlation function,

$$S_\rho(q) = \frac{1}{2\pi}\int_{-\infty}^{\infty} S_\rho(q,\omega)\mathrm{d}\omega = F_\rho(q,t=0), \tag{13}$$

where $S_\rho(q,\omega)$ is the power spectrum (dynamic structure factor[4]) of $F_\rho(q,t)$. Such peaks are not present in the correlation times from the UA simulations. The peaks show that there is a strong tendency in the MARTINI force field for the lipid molecules to cluster at these distances, leading to slowing-down of the relaxation.

C. Modeling the relaxation with a stretched exponential

The question is now whether a model function can be found that fits to the correlation functions calculated from simulation data and captures the physics of the relaxation processes. Weight is put on a model function with as few parameters as possible that still has a minimal fit error according to Eq. (11). The starting point is the observation that the correlation functions decay slower-than-exponential (Fig. 2), ruling out the conventional single-exponential form. The first model function candidate would perhaps be two or several exponential functions. This is certainly a viable choice and the physical interpretation would be a number of different modes relaxing by different processes (preferably on different time scales). However, two reasons make the fit of a superposition of exponential functions to simulation data suboptimal. First, this requires more parameters for the free fit (the number increases with two for every exponential added and is to be kept to a minimum). Second, and most important in this case, the relaxation data show no distinct plateaus that would be the sign of different relaxation processes, but are smoothly and monotonically decreasing functions toward zero.

Another common and plausible choice for the model function of slow relaxation is an (inverse) power-law. A power-law diverges as $t \to 0$ and can obviously not be correct on the shortest timescales. This problem can be circumvented using the general form,

$$F(q,t) = \frac{F(q,0)}{1 + a_0(q)t^{a_1(q)}}. \tag{14}$$

The long-time behavior of this function, the inverse power-law $F(q,t) \sim t^{-a_1(q)}$ gives a linear curve when plotted in double logarithmic scales, with $a_1(q)$ as the negative line slope. Simulation data show no clear linear relation. Admittedly, a power-law-fit could be done at least for partial times, but is really not a satisfactory solution for the entire time domain. In any case, the best power-law that could be fitted to the correlation functions was $a_1 \approx 1$ for the UA simulations and $a_1 \approx 1.2$ for the CG simulations. These numbers were fairly constant over the wave vector domain (data not shown).

A plot of $\ln(-\ln(F(q,t)))$ against $\ln(t)$ shows a strikingly linear relationship (Fig. 6) that prevails over basically the

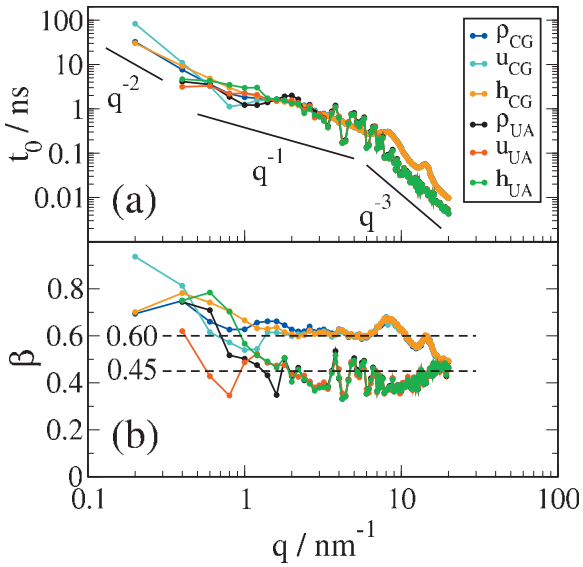

FIG. 7. Free-fit parameters for the stretched exponential: (a) $t_0(q)$ and (b) $\beta(q)$. Times are reported in the physical timescale.

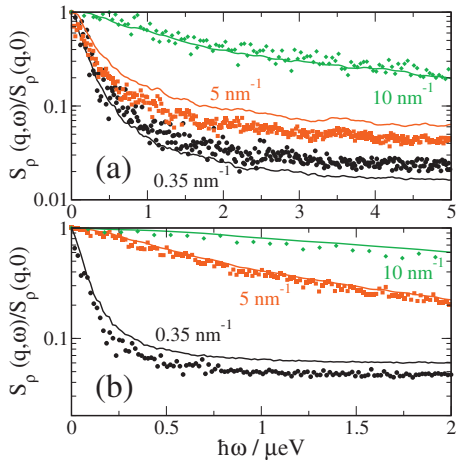

FIG. 8. Power spectra of the density-density correlation function. The filled circles are raw simulation data and the solid lines are simulation data convolved with a Lorentzian window function, $f(\omega)=2\sigma/(\omega^2+\sigma^2)$, alias effects broadens the high frequencies. For the wave vectors $q=\{0.35,5,10\}$ nm^{-1}, the windows used were $\sigma=\{0.026,0.026,0.066\}$ μeV for (a) the UA simulations and $\sigma=\{0.0026,0.26,1.32\}$ μeV for (b) the CG simulations. The results were not sensitive to these numbers as long as small σ-values were used. Note the different energy scales in (a) and (b).

entire time domain (as long as the statistics is sufficient) for all available wave vectors (0.2–20 nm^{-1}). This is characteristic for a stretched exponential function,

$$F(q,t)=F(q,0)e^{-(t/t_0(q))^{\beta(q)}}. \tag{15}$$

The shape [if normalized according to $F(q,t)/F(q,0)$] is determined by two parameters, $t_0(q)$ and $\beta(q)$, that are free to depend on the wave vector q. t_0 is a parameter with dimension time that measures the length of the correlations, while $0<\beta<1$ is a dimensionless parameter called the stretching exponent, that determines to which degree the stretching prevails. A small value of β makes the nonexponential tail of the decay longer, while $\beta=1$ corresponds to ordinary exponential decay.

With this strictly empirical form to fit data, very good agreement was found over all domains of the wave vector and most of the time domain (Figs. 2 and 6). Deviations from the stretched exponential behavior are most noticeable for the shortest times (<0.1 ns), which we have not analyzed in detail anyway (as it relates to vibrational relaxation as explained previously). For a stretched exponential the correlation time defined in Eq. (7) becomes

$$\tau=2\int_0^\infty \frac{[F(q,t)]^2}{[F(q,0)]^2}\mathrm{d}t=2\int_0^\infty e^{-2(t/t_0)^\beta}\mathrm{d}t. \tag{16}$$

The substitution $x=2(t/t_0)^\beta$ gives

$$\tau=\frac{2}{2^{1/\beta}}\frac{t_0}{\beta}\int_0^\infty e^{-x}x^{1/\beta-1}\mathrm{d}x=2^{(\beta-1)/\beta}\frac{t_0}{\beta}\Gamma\left(\frac{1}{\beta}\right), \tag{17}$$

where the integral representation of the gamma function[54] has been used. The relaxation time is finite for all $\beta>0$. Regardless of how stretched the exponential is, a finite (although sometimes very large) correlation time is obtained. A fit of simulation data to Eq. (15) was performed with the two free parameters $t_0(q)$ and $\beta(q)$; they are shown in Fig. 7 as functions of the wave vector. The time parameter, t_0, follows very closely the shape of the correlation time τ (Fig. 3), underlining the agreement of the stretched exponential fit to the simulation data. Since t_0 is proportional to τ, the same power-law behaviors apply to t_0; up to $q_c\approx 5$ nm^{-1} we find a q^{-1} relation, which then crosses over to q^{-3} behavior (Figs. 3 and 7). The stretching exponent β is only weakly dependent on q but increases for the smallest wave vectors. The two force fields give slightly different stretching, $\beta\approx 0.45$ for the UA and $\beta\approx 0.60$ for the CG simulations. In the CG data, the static structure factor peaks that are present in the correlation time (and time parameter t_0) are also present in β. The UA simulations give a remarkably q-independent β, while the stretching exponent from the CG simulations decreases somewhat with q. The stretching exponents seem to converge around 0.5 for the largest wave vector, $q=20$ nm^{-1}, for both models.

We have also calculated the power spectra (dynamic structure factors) $S(q,\omega)$ for the time correlation functions $F(q,t)$. The two functions are related by a time Fourier transform,

$$S(q,\omega)=\int_{-\infty}^{\infty}\mathrm{d}t e^{-i\omega t}F(q,t), \tag{18}$$

and subsequently contain the same information, although the long-time (low frequency) information is usually better visualized in the time domain and vice versa. Some representative power spectra for the number density are shown in Fig. 8. Remembering that the Fourier transform of an exponential function is a Lorentzian function, the power spectrum corresponding to exponential decay is

$$S(q,\omega)=\frac{2\tau(q)}{1+(\tau(q)\omega)^2}. \tag{19}$$

For a stretched decay there is no analytic expression for the transform (except for very few special cases, e.g., $\beta=0.5$, see Ref. 55) but a numerical transform can always be carried out.

TABLE II. Goodness-of-fits of $F_\rho(q,t)$ sorted by best fit functions in descending order. The second column lists the number of free fit parameters, while the third and fourth columns report the mean value of $\epsilon_{mf}(q)$, defined in Eq. (11), compared to the value obtained for the stretched exponential model function. The fits were made in the q-domain 0.3–20 nm^{-1}, separately for the UA and CG simulation data, and the correlation functions were used until they had decreased to 5% of their initial values.

		$\langle\epsilon_{mf}\rangle/\langle\epsilon_{stretched}\rangle$	
Model function	Parameters	UA	CG
Stretched exponential	2	1.00	1.00
Double exponential	3	1.81	3.34
Inverse power-law[a]	2	3.46	29.45
Single exponential	1	21.86	98.76

[a]The power exponents obtained from the best fits were $a_1=1$ and $a_1=1.2$ for the UA and CG simulations, respectively.

We note that stretching introduces a characteristic difference to the power spectra. The broader extension in the time domain corresponds to a more narrow decay; the spectrum is shifted to lower frequencies. For the higher frequencies, corresponding to the shorter times, the spectra are comparable to that of the Lorentzian spectrum (single-exponential decay).

We conclude this section with a discussion of the accuracy of the fits to the different model functions. With the residual fit-error defined in Eq. (11) as a measure of the goodness-of-fit, we have compared a number of model functions to the stretched exponential. The results are compiled in Table II. The wave vector-dependence of $\epsilon_{mf}(q)$ is relatively weak, so we have chosen to give its mean value. The conclusions hold equally well for other representative measures as well. A typical example of how a fit looks is shown in Fig. 9, at $q=3$ nm^{-1}, a value where $\epsilon_{mf}(q)$ is very close to its mean value. The stretched exponential gives the smallest fit error, and also the double exponential is clearly superior to the inverse power-law and, in particular, to the single-exponential. In addition to the smallest $\epsilon_{mf}(q)$, two major facts favor the stretched exponential fit. First, it contains the fewest free parameters (two instead of three for the double exponential) and still reproduces data best. Second, it is linear in a plot of $\ln(-\ln(F(q,t)))$ versus $\ln(t)$ as characteristic for the stretched exponential, while double logarithmic plots showed no distinct plateaus, which would be characteristic for two exponentials having time constants on separate time scales.

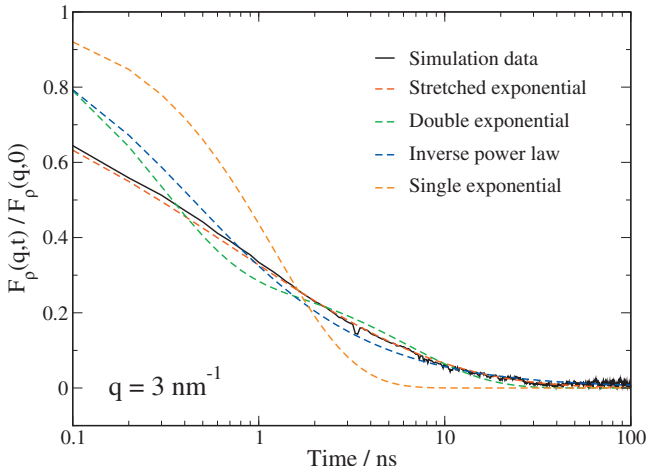

FIG. 9. Goodness-of-fit of $F_\rho(q,t)$ for the UA simulations at $q=3$ nm^{-1}. The solid black line is the simulation data and the dashed lines are the model functions listed in Table II, fitted to simulation data. Times are reported in the physical time scale.

V. DISCUSSION

The bilayer molecular structure influences the relaxation dynamics of almost all wave vectors accessible to the simulations. More precisely, the in-plane number density fluctuations dominate down to a characteristic wave vector $q_0 \approx 2$ nm^{-1}; this number corresponds very closely to the distance where the radial distribution function $g(r)$ starts to separate from 1 (Fig. 5). Wave vectors above q_0 involve the dynamics of a single, up to a few, lipids. In the vicinity of q_0 the dynamics is a combination of bulk and interface fluctuations. For $q \ll q_0$, fluctuations in the bulk and in the interface are expected to decouple but this cannot be seen in the simulation data. The hydrodynamic limit behavior is not clear from studying even the lowest q-modes, e.g., at $q=0.3$ nm^{-1} the correlation times for neither force field show the divergent behavior characteristic to hydrodynamic fluctuations. Although at $q=0.2$ nm^{-1}, a mode that is reached only in the CG simulations $\tau(q)$ has increased substantially. We find a crossover between two power-laws around $q_c=5$ nm^{-1}, with $\tau \propto q^{-1}$ for the lower wave vectors and $\tau \propto q^{-3}$ for the higher wave vectors. We note that the crossover wave vector is close to the interlipid distance and hence suggest that it interpolates between the single lipid dynamics regime and the collective regime where several lipids interact in the relaxation process. The correlation functions $F(q,t)$ are excellently described by stretched exponential functions, with a weakly q-dependent stretching exponent β and a time parameter t_0 that closely match the correlation time. Because the number density fluctuations are dominant over most of the wave vector regime, the stretched behavior is a feature of the structure of the two-dimensional fluid bilayer. This is also expressed by that the stretching exponent tends to increase toward unity for the short wave vectors, which is consistent with the ordinary exponential behavior expected in the hydrodynamic limit.

Experiment and simulation data may be interpreted within the frameworks of several different theories, which all

try to predict dispersion relations (relations between wave vector and decay rate) for the membrane shape fluctuations. There are theories that target both undulations and (number) density fluctuations, although to our knowledge no dynamic fluctuation theory has been presented for thickness fluctuations. In principle that could easily be done in the same way as for classical undulation theory with few if any complications. In this discussion, we will focus on $F_\rho(q,t)$ since the number density fluctuations are dominant over most of the wave vector regime of the simulations.

A particular theory that has drawn attention the last decade is Zilman–Granek (ZG) theory[25,26] which actually predicts a stretched exponential for the intermediate scattering function,

$$F_\rho(q,t) = F_\rho(q,0)e^{-(t/t_0(q))^{2/3}}, \tag{20}$$

with dispersion relation,

$$t_0^{-1}(q) = 0.025\gamma_k\left(\frac{k_BT}{k_c}\right)^{1/2}\frac{k_BT}{\eta}q^3$$

and stretching exponent

$$\beta = 2/3. \tag{21}$$

γ_k is a numerical factor close to unity and k_BT the product of the Boltzmann constant and the absolute temperature, as usual. Two material properties enter the dispersion relation; k_c is the membrane bending rigidity and η is the bulk viscosity of the solvent. NSE experiments are usually interpreted within ZG theory since the time and lengths scales covered by experiments and theory are roughly the same. The agreement with NSE data in the investigated q-domains is, in general, favorable, but a known shortcoming is that ZG theory gives too large values for k_c. Even before ZG theory, Farago and co-workers had introduced an "effective" viscosity four to six times higher than the bulk viscosity in help to fit NSE data.[56] Other experimental groups have followed this route and modified the η in the ZG theory in the same way to obtain agreement.[16,17,57,58] As a more rigorous attempt to explain the high k_c-values, Watson and Brown[59] have proposed that the underlying hydrodynamic assumption in ZG theory is inadequate and that a more accurate hydrodynamic description due to Seifert and Langer,[21,22] which includes monolayer friction, leads to a rescaled, effective, bending rigidity in the ZG dispersion relation, Eq. (21). In any case, the molecular structure of the bilayer is not included in ZG theory at all, and the theory cannot be expected to describe the bilayer dynamics for wave vectors comparable to 2π times the inverse membrane thickness and longer. A recent NSE experiment that reaches such wave vectors has shown these type of deviations.[16]

The simulation data can be fitted quite well to a ZG equation, i.e., a stretched exponential with $\beta=2/3$ although a slightly smaller exponent gives better agreement. The dispersion relation obtained from this does, however, not have the q^{-3} shape predicted by Eq. (21) over the entire q-interval covered by the simulations, but only for the higher wave vectors (above 5 nm^{-1}). See Fig. 10 for the correlation times versus wave vector. It is clear that the slope in this double logarithmic diagram is close to -3 at the high end, while it is closer to -1 or -2 in the low q end. The numerical value for $t_0(q)$ agrees in the high-q end with the prediction from Eq. (21) if we put $\gamma_k=1$, use $k_c=7\times10^{-20}$ J (which is the value obtained from the present type of UA simulations[60] and the latest experimental value[34]) and a 2.5 times too large value, $\eta=2.0\times10^{-3}$ Pa s for the water viscosity. It is quite conceivable that the viscosity of the thin water sheet in the lipid head groups region is higher than that of bulk water. It is noteworthy that similar values for the viscosity of the water around the lipid bilayer are obtained from a calculation of the water/lipid bilayer friction in simulations.[10] This is also the same type of effective viscosity as discussed for the experiments above, although the scaling factor is slightly smaller. The lower wave vectors cross over to a q^{-1} line as we have stated earlier, and for the CG data q^{-2} behavior starts to set in for the lowest modes, although this is somewhat uncertain considering the limited number of points in the low q-domain. Thus, we conclude that there is a clear disagreement between the present simulations and the ZG theory as well as experiments below about 5 nm^{-1}. The simulation data of Flenner and co-workers[20] are only shown above 3 nm^{-1} in Fig. 10, but their data go down to 1 nm^{-1} in the cited article and seem to agree better with our data than with NSE-experiments or the ZG-theory.

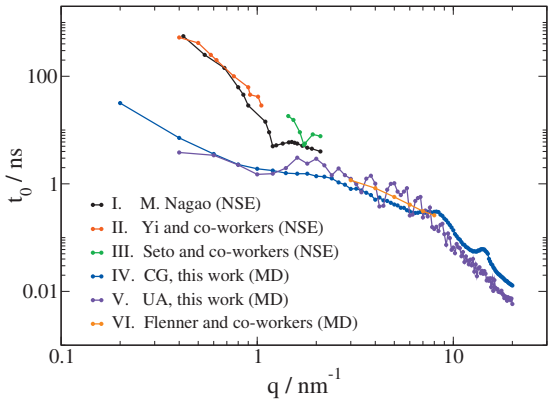

FIG. 10. Comparison of correlation times in the ZG model as fitted to a stretched exponential with $\beta=2/3$. The solid lines are guides to the eye. Data from (I) Fig. 3 in Ref. 16, (II) Fig. 4(a) in Ref. 17, (III) Fig. 8 in Ref. 15, (IV) CG simulation data from the present work, (V) UA simulation data from the present work, (VI) Fig. 8 in Ref. 20, a subset of data was chosen where β is close to 2/3.

One may ask whether a fit to a Seifert–Langer theory (two exponentials) would work better. It is, however, clear that the time dependence of such a correlation function does not fit the simulations (see Fig. 9). This is even more problematic if one of the amplitudes is quite small as indicated in Ref. 19. The q-dependence of both the correlation times switches in the Seifert–Langer theory between q^{-2} and q^{-3} which would give a change in the correlation times with four to six orders of magnitude over the q-interval 0.1–10 nm^{-1}, while the simulations indicate a change by about three orders of magnitude over that interval. The correlation times in the Seifert–Langer theory depend on a number of parameters. Most of these have well known values that agree reasonably between simulation and experiment, but one of them, the intermonolayer friction, differs by two orders of magnitude between simulations and experiment,[13,19] probably due to

TABLE III. Setups of recent experiment and simulation studies. The last column lists the q-domain where data have been fitted to a stretched exponential with exponent of 2/3, as available from the published data.

No.	Study	Sample	Method	q (nm^{-1})
I	Nagao[a]	$C_{12}E_5/C_8D_{18}$	NSE	0.4–2.1
II	Yi and co-workers[b]	PC[c]	NSE	0.4–1.0
III	Seto and co-workers[d]	PC[e]	NSE	1.4–2.1
IV	Present work (CG)	PC[f]	MD	0.2–20.0
V	Present work (UA)	PC[g]	MD	0.3–20.0
VI	Flenner and co-workers[h]	PC[g]	MD	3.0–8.0

[a]Reference 16.
[b]Reference 17.
[c]Unilamellar vesicles of PC:s in the range 14–20 with and without an unsaturated bond.
[d]Reference 15.
[e]Stacked DMPC (14:0) and DPPC (18:0).
[f]Single-layer DLPC (12:0).
[g]Single-layer DMPC (14:0).
[h]Reference 20.

differences in length scale between simulations and experiment. Using the experimental value gives at $q=1$ nm^{-1} the two correlation times of 0.5 and 0.01 ns, while the use of the intermonolayer friction from the united-atom lipid simulations[13] gives the time constants of 0.13 and 0.012 ns. This should be compared to the correlation time calculated from the simulations which is 2.5 ns at this q-value. At $q=0.3$ nm^{-1} the corresponding correlation times are about 5 and 0.4 ns (with smaller differences depending on which value that is used for the monolayer friction). This is closer to the simulations (15 ns). Since the q-dependence is stronger in the Seifert–Langer theory than in the simulations, the correlation times will approach each other at still lower q-values. This indicates perhaps that one has to go to still lower q-values before the Seifert–Langer theory is valid.

For further investigation and a clear comparison to the experimental situation, in Fig. 10 we have compiled data on similar bilayer systems from different NSE experiments and another MD study. Details about these studies can be found in Table III. Our data overlap excellently with the MD data from Flenner and co-workers[20] which was done on an all-atom model (the CHARMM27 force field[61]). They only calculated the incoherent intermediate scattering function, while our data also include the collective dynamics. The data should be comparable at least on an order-of-magnitude scale anyway. Since they used β as a free-fit parameter, we have chosen a subset of their data where β is close to 2/3, but also for the lower wave vectors their data show the same type of faster decay as ours. The experimental data are similar between the three NSE studies but orders of magnitude slower for the low wave vectors compared to MD data. The NSE data fit remarkably well to the q^{-3} behavior of the high wave vectors of our data but that is only an extrapolation since the NSE experiments do not reach that long wave vectors. On the short length scales, conventional neutron scattering or x-ray scattering is the main source of experimental data. Rheinstädter and co-workers[62] have found deviations from single-exponential behavior also in this regime, but interpreted their data in terms of the double exponential model function. Given our MD data that cover a broad range of mesoscopic wave vectors, it would be interesting to reanalyze these data in light of a stretched exponential model function. Visual inspection of the intermediate scattering function at $q=14$ nm^{-1} [Fig. 3(c) in Ref. 62] shows a decay that is the same order of magnitude compared to our data. MD data and experiment data agree on molecular length scales but differ closer to the hydrodynamic limit. The different results are likely to be explained by the difference in setup between experiments and simulations.

The simulated systems consist of one bilayer that is periodically repeated in the direction perpendicular to the bilayer. The water content (23 waters per lipid) is large enough not to affect the equilibrium properties of the bilayer by dehydration, and an additional simulation of the CG 8192-lipid system, with 200 waters per lipid, showed the same dynamics with unchanged correlation times for the longest wavelengths. Still the water layer between the periodically repeated 3.6 nm thick lipid bilayer is 2.4 nm for the UA 1024-lipid system. This differs from the stacked systems or micelles studied experimentally. For the stacked systems one could imagine that different shapes of the stacked bilayers could slow down the dynamics compared to a system where all the stacked bilayers are shaped in exactly the same way. Micellar systems differ also clearly from the presently simulated systems although it is less clear what the precise reason for a difference in the dynamics could be in that case. The presence of even a very small surface tension is also something that could cause a slowing down of the dynamics. Although the explanation may be related to a difference in experimental and simulation setups, the difference in relaxation rate of one to two orders of magnitude between simulations and NSE for wave vectors below $1-2$ nm^{-1} remains to explained. This also means that the simulations disagree with the ZG theory in the low wave vector region where a field theory could be expected to work well. On the contrary, the ZG theory and the simulations agree quite well for high wave vectors, where a field theory could be close the limit of its validity.

VI. CONCLUSIONS

We have used molecular dynamics simulations to study the dynamics of lipid bilayer over a broad range of meso- and microscopic wave numbers. Simulation data cover the domain $0.2<q<20$ nm^{-1} $(0.3<\lambda<30$ nm), with correlations in the time range $0<t<1$ μs. Results from both the UA and CG force fields are in quantitative agreement if the CG data are scaled with a factor $\alpha_t=10$ to account for the faster CG dynamics due to the smoother free energy landscape. Understanding the influence of fluctuations on different length- and timescales can help in the construction of new molecular models of the lipid bilayer, as well as the interpretation of experimental data. With molecular simulations on different levels of detail, this paper has separated the fluctuation contributions from in-plane (density) and out-of-plane (thickness and undulation) fluctuations.

The time correlation functions of structure fluctuations in the bilayer are stretched exponentials. The time parameter

in the stretched exponentials follows two different power-laws with a crossover at a wave vector close to the lipid neighbor distance. The stretching exponent is only weakly q-dependent and slightly different for the two force fields. We find $\beta=0.45$ for the UA simulations and $\beta=0.6$ for the CG simulations. These numbers are both slightly smaller than the stretching exponent predicted by ZG theory, $\beta=2/3$. The effect of the molecular structure is pronounced for all wave vectors and height fluctuations are only apparent for the lowest wave vectors, below 1 nm^{-1}. The CG model shows prominently more structure than the UA model at distances that coincide with the peak positions of the static structure factor.

Our data agree with earlier MD work and experimental data at high wave vectors. However, we do not find agreement with NSE data at low wave vectors, where a faster relaxation than in the NSE experiments is observed. At higher wave vectors the dispersion relations follow two different power-laws, with exponents $\tau \propto q^{-1}$ and $\tau \propto q^{-3}$. The crossover takes place at $q_c=5$ nm^{-1}.

ACKNOWLEDGMENTS

This work has been supported by SNIC (Swedish National Infrastructure for Computing) with computer time at HPC2N—High Performance Computing Center North and has been funded by the Swedish Science Research Council (VR) with a grant to OE.

[1] L. van Hove, Phys. Rev. **95**, 249 (1954).
[2] J. P. Hansen and I. R. McDonald, *Theory of Simple Liquids*, 3rd ed. (Academic, New York, 2006).
[3] D. Forster, *Hydrodynamic Fluctuations, Broken Symmetry, and Correlation Functions* (Perseus Books, New York, 1990), Chap. 4.
[4] J. P. Boon and S. Yip, *Molecular Hydrodynamics* (McGraw-Hill, New York, 1980).
[5] R. D. Mountain, J. Res. Natl. Bur. Stand., Sect. A **70A**, 207 (1966).
[6] C. J. Montrose, V. A. Solovyev, and T. A. Litovitz, J. Acoust. Soc. Am. **43**, 117 (1968).
[7] C. Demoulin, C. J. Montrose, and N. Ostrowsky, Phys. Rev. A **9**, 1740 (1974).
[8] U. Bafile, E. Guarini, and F. Barocchi, Phys. Rev. E **73**, 061203 (2006).
[9] S. Safran, *Statistical Thermodynamics of Surfaces, Interfaces, and Membranes* (Westview, Boulder, 2003).
[10] O. Edholm, in *Computational Modeling of Membrane Bilayers, Current Topics in Membranes*, edited by S. E. Feller (Academic, New York, 2008), Vol. 60, Chap. 3, pp. 91–110.
[11] M. F. Brown, A. A. Ribeiro, and G. D. Williams, Proc. Natl. Acad. Sci. U.S.A. **80**, 4325 (1983).
[12] E. Lindahl and O. Edholm, J. Chem. Phys. **115**, 4938 (2001).
[13] J. Wohlert and O. Edholm, J. Chem. Phys. **125**, 204703 (2006).
[14] E. G. Brandt and O. Edholm, Biophys. J. **96**, 1828 (2009).
[15] H. Seto, N. L. Yamada, M. Nagao, M. Hishida, and T. Takeda, Eur. Phys. J. E **26**, 217 (2008).
[16] M. Nagao, Phys. Rev. E **80**, 031606 (2009).
[17] Z. Yi, M. Nagao, and D. P. Bossev, J. Phys.: Condens. Matter **21**, 155104 (2009).
[18] S. A. Shkulipa, W. K. den Otter, and W. J. Briels, Phys. Rev. Lett. **96**, 178302 (2006).
[19] S. A. Shkulipa, W. K. den Otter, and W. J. Briels, J. Chem. Phys. **125**, 234905 (2006).
[20] E. Flenner, J. Das, M. C. Rheinstädter, and I. Kosztin, Phys. Rev. E **79**, 011907 (2009).
[21] U. Seifert and S. A. Langer, Europhys. Lett. **23**, 71 (1993).
[22] U. Seifert and S. A. Langer, Biophys. Chem. **49**, 13 (1994).
[23] E. Evans and A. Yeung, "Functional dynamics of lipids in biomembranes," special issue of Chem. Phys. Lipids **73**, 39 (1994).
[24] A. Yeung and E. Evans, J. Phys. II **5**, 1501 (1995).
[25] A. G. Zilman and R. Granek, Phys. Rev. Lett. **77**, 4788 (1996).
[26] A. G. Zilman and R. Granek, Chem. Phys. **284**, 195 (2002).
[27] M. Doi and S. F. Edwards, *The Theory of Polymer Dynamics*, International Series of Monographs on Physics Series No. 73 (Oxford University Press, Oxford, 1986).
[28] M. D. Ediger, C. A. Angell, and S. R. Nagel, J. Phys. Chem. **100**, 13200 (1996).
[29] J. C. Dyre, Rev. Mod. Phys. **78**, 953 (2006).
[30] R. Zwanzig and N. K. Ailawadi, Phys. Rev. **182**, 280 (1969).
[31] D. Frenkel and B. Smit, *Understanding Molecular Simulation: From Algorithms to Applications* (Academic, San Diego, CA, 1996).
[32] M. P. Allen and D. J. Tildesley, *Computer Simulation of Liquids* (Oxford University Press, New York, 1989).
[33] R. H. Pearson and I. Pascher, Nature (London) **281**, 499 (1979).
[34] N. Kucerka, Y. Liu, N. Chu, H. I. Petrache, S. Tristram-Nagle, and J. F. Nagle, Biophys. J. **88**, 2626 (2005).
[35] O. Berger, O. Edholm, and F. Jähnig, Biophys. J. **72**, 2002 (1997).
[36] S. J. Marrink, A. H. de Vries, and A. E. Mark, J. Phys. Chem. B **108**, 750 (2004).
[37] S. J. Marrink, H. J. Risselada, S. Yefimov, D. P. Tieleman, and A. H. de Vries, J. Phys. Chem. B **111**, 7812 (2007).
[38] L. Monticelli, S. K. Kandasamy, X. Periole, R. G. Larson, D. P. Tieleman, and S.-J. Marrink, J. Chem. Theory Comput. **4**, 819 (2008).
[39] H. J. C. Berendsen, J. P. M. Postma, W. F. van Gunsteren, and J. Hermans, in *Intermolecular Forces*, edited by B. Pullman (D. Reidel, Dordrecht, 1981), pp. 331–342.
[40] E. Lindahl and O. Edholm, Biophys. J. **79**, 426 (2000).
[41] B. Hess, C. Kutzner, D. van der Spoel, and E. Lindahl, J. Chem. Theory Comput. **4**, 435 (2008).
[42] B. Hess, J. Chem. Theory Comput. **4**, 116 (2008).
[43] T. Darden, D. York, and L. Pedersen, J. Chem. Phys. **98**, 10089 (1993).
[44] U. Essmann, L. Perera, M. L. Berkowitz, T. Darden, H. Lee, and L. G. Pedersen, J. Chem. Phys. **103**, 8577 (1995).
[45] S. Nosé, Mol. Phys. **52**, 255 (1984).
[46] W. G. Hoover, Phys. Rev. A **31**, 1695 (1985).
[47] M. Parrinello and A. Rahman, J. Appl. Phys. **52**, 7182 (1981).
[48] S. Nosé and M. L. Klein, Mol. Phys. **50**, 1055 (1983).
[49] M. Frigo and S. G. Johnson, "Program generation, optimization, and platform adaptation" special issue of Proc. IEEE **93**, 216 (2005).
[50] K. Levenberg, Q. Appl. Math. **2**, 164 (1944).
[51] D. Marquardt, SIAM J. Appl. Math. **11**, 431 (1963).
[52] M. I. A. Lourakis, "levmar: Levenberg-marquardt nonlinear least squares algorithms in C/C++," http://www.ics.forth.gr/~lourakis/levmar (December 2009), (Accessed on 10 Feb. 2010).
[53] J. G. Powles, D. M. Heyes, G. Rickayzen, and W. A. B. Evans, J. Chem. Phys. **131**, 214509 (2009).
[54] P. J. Davis, in *Handbook of Mathematical Functions with Formulas, Graphs, and Mathematical Tables*, Applied Mathematics Series No. 55, edited by M. Abramowitz and I. A. Stegun (National Bureau of Standards, Washington, D.C., 1964), Chap. 6, p. 255.
[55] M. N. Berberan-Santos, E. N. Bodunov, and B. Valeur, Chem. Phys. **315**, 171 (2005).
[56] B. Farago, M. Monkenbusch, K. D. Goecking, D. Richter, and J. S. Huang, Physica B **213–214**, 712 (1995).
[57] T. Takeda, Y. Kawabata, H. Seto, S. Komura, S. K. Ghosh, M. Nagao, and D. Okuhara, J. Phys. Chem. Solids **60**, 1375 (1999).
[58] S. Komura, T. Takeda, Y. Kawabata, S. K. Ghosh, H. Seto, and M. Nagao, Phys. Rev. E **63**, 041402 (2001).
[59] M. C. Watson and F. L. H. Brown, Biophys. J. **98**, L9 (2010).
[60] Q. Waheed and O. Edholm, Biophys. J. **97**, 2754 (2009).
[61] S. E. Feller and A. D. MacKerell, J. Phys. Chem. B **104**, 7510 (2000).
[62] M. C. Rheinstädter, T. Seydel, and T. Salditt, Phys. Rev. E **75**, 011907 (2007).